IOP Publishing Journal of Physics: Condensed Matter
J. Phys.: Condens. Matter **25** (2013) 095007 (8pp) doi:10.1088/0953-8984/25/9/095007

Rubber friction for tire tread compound on road surfaces

B Lorenz[1,3], B N J Persson[1,3], G Fortunato[2], M Giustiniano[2] and F Baldoni[2]

[1] IFF, FZ-Jülich, D-52425 Jülich, Germany, EU
[2] Bridgestone Technical Center Europe S.p.A., Tire Research Department, Wear & Durability Group, Via del Fosso del Salceto 13/15 00129, Rome

E-mail: b.lorenz@fz-juelich.de

Received 26 October 2012, in final form 27 December 2012
Published 18 January 2013
Online at stacks.iop.org/JPhysCM/25/095007

Abstract
We have measured the surface topography and calculated the surface roughness power spectrum for an asphalt road surface. For the same surface we have measured the friction for a tire tread compound for velocities 10^{-6} m s^{-1} $< v <$ 10^{-3} m s^{-1} at three different temperatures (at −8 °C, 20 °C and 48 °C). The friction data was shifted using the bulk viscoelasticity shift factor a_T to form a master curve. We have measured the effective rubber viscoelastic modulus at large strain and calculated the rubber friction coefficient (and contact area) during stationary sliding and compared it to the measured friction coefficient. We find that for the low velocities and for the relatively smooth road surface we consider, the contribution to friction from the area of real contact is very important, and we interpret this contribution as being due to shearing of a very thin confined rubber smear film.

(Some figures may appear in colour only in the online journal)

1. Introduction

Rubber friction is a topic of huge practical importance, e.g., for tire applications [1–20]. However, it is also a topic of great complexity. In this paper we present the results of a rubber friction study for a tread rubber block sliding at low velocity on an asphalt road surface. The present study complements the study presented in [21] which focused on two model rubbers, namely unfilled and filled (with carbon black) Styrene–Butadiene (SB) rubber. Earlier studies of rubber friction on rough surfaces indicate that there are several contributions to rubber friction [14, 21, 22], and we believe that only from a detailed study of several different systems (different types of rubber and substrate surfaces) under different sliding conditions (velocity and temperature) will it be possible to gain a quantitative insight into the relative importance of the various contributions to rubber friction.

Consider a rubber block sliding on a hard rough substrate, say a road surface. The road asperities will induce pulsating deformations of the rubber, resulting in viscoelastic energy dissipation in the bulk of the rubber which gives an important contribution to the friction [5]. The viscoelastic deformations involve very large strain, typically of order ∼100%, and in order to correctly describe the viscoelastic deformations and (more important) the area of contact between the road and the rubber, it is necessary to measure the viscoelastic properties at large strain. In this paper (section 4) we describe a new procedure for obtaining the large-strain modulus to be used, e.g., in rubber friction applications. In addition to the viscoelastic contribution to the friction there will be a contribution from the area of contact. In this paper we find that the frictional shear stress which acts in the area of contact is likely due to shearing a thin confined fluid or rubber smear film, which results in a weakly velocity-dependent shear stress [23, 24][4], [26]. In [21] we found a similar contribution to the friction for unfilled SB-rubber, while for filled SB-rubber we have found a frictional shear stress which depended strongly on the sliding velocity, and which we interpreted as due to adhesive opening cracks at the exit side of the asperity contact regions [27–29]. In addition to these processes there may be a contribution to the friction from

[3] www.MultiscaleConsulting.com.

[4] Yew *et al* [25] have shown that when sliding polymer-on-polymer systems, the shear deformation is localized to a band about 3 nm thick at the interface of the polymer surfaces.

rubber wear. For dirty tires, e.g., tread blocks covered by sand particles, no direct rubber–road contact may occur, and in this case there will be a (nearly velocity independent) contribution to the friction from sliding of the (hard sand) particles against the road surface.

As the rubber–road interface is studied at increasing magnification, new smaller-scale roughness will be observed on the road surface and the stress in the apparent contact regions between the rubber and the road will increase. During sliding, at short enough length scale (observed at high enough magnification), the shear stress (and the temperature) in the contact regions will finally be so high as to start to rupture chemical bonds in the surface region of the rubber. This will result in a thin (typically micrometer thick) surface layer of rubber with modified properties, which we refer to as the wear layer. The viscoelastic contact mechanics model cannot be used at length scales smaller than the thickness of the wear layer. We therefore define the area of contact between the rubber and the road surface as the area of contact at the point where one reaches the length scales given by the thickness of the wear layer. The frictional shear stress acting in the area of contact is therefore an effective shear stress associated with the contact between a rather ill-defined rubber layer and the road surface. It is clear that only a combined experimental–theory approach can determine the nature of the frictional shear stress acting in the area of contact. We will discuss this topic again in section 3.

This paper is organized as follows. In section 2 we describe how we have determined the road surface topography and the viscoelastic modulus of the rubber at large strain. We also describe the setup used in the rubber friction experiment. In section 3 we briefly review the theoretical picture used to analyze the rubber friction experiment. Section 4 presents combined experimental–theory results for the large-strain viscoelastic modulus of the tread rubber used in our study. In section 5 we present the measurements of rubber friction and the theoretical analysis of the experimental data. Section 6 presents a discussion and section 7 the summary and conclusions.

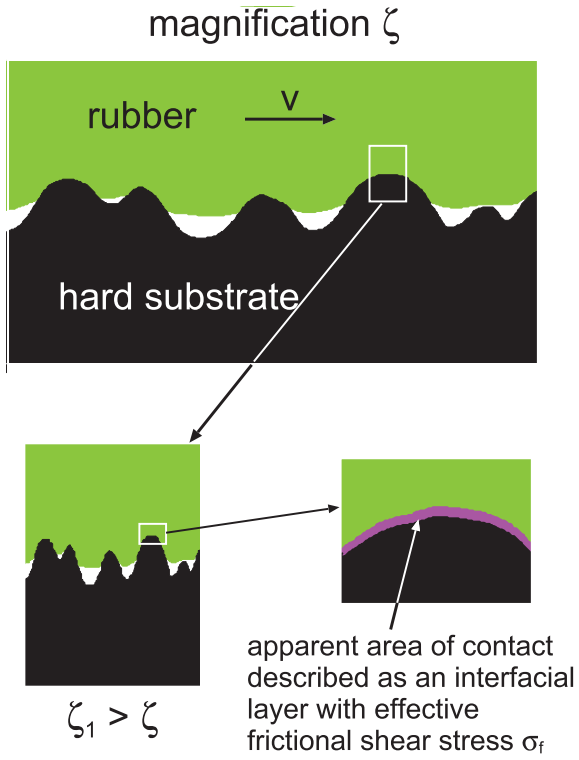

Figure 1. The basic picture used in analyzing the rubber friction problem: Many length scales are involved and the friction has contributions from all the length scales. The viscoelastic contribution to the friction arises from the (time-dependent) deformations of the rubber by the asperities which can be observed as the magnification increases up to the cut-off ζ_1. When the contact regions are observed at magnification larger than ζ_1 the interfacial stress (and temperature) becomes so high that highly non-linear processes, such as bond breaking and wear processes, will occur, which cannot be described using continuum (viscoelastic) theory, but which may require an atomistic approach. These regions are indicated by the pink area in the figure. The effective frictional shear stress which acts in these regions are denoted by τ_f and will in general depend on the sliding velocity and the temperature. Understanding the origin of τ_f may require insight into the bond breaking (wear) and other atomistic processes occurring in the apparent contact area (see figure 2).

2. Experimental details

The friction coefficient has been measured by sliding a rectangular (2×2 cm^2), 5 mm thick rubber block in a translatory motion over a road surface as described in section 3 in [21]. The rubber is a tread compound used on summer tires for passenger cars. The nominal load on the rubber sample was 26 N, resulting in the nominal squeezing pressure $\sigma_0 = 0.065$ MPa. When a stable friction value is reached after run-in, the friction force and thus the friction coefficient is measured at a constant velocity. The velocity is changed in steps, starting at about 10^{-3} m s^{-1} and ending at about 10^{-6} m s^{-1}. We then change the temperature and repeat the whole procedure. For the following analysis we have measured friction curves at three different temperatures (at $-8\,^\circ$C, $20\,^\circ$C and $48\,^\circ$C). The results are then shifted [30] along the velocity axis using the measured (in the dynamic mechanical analysis of the rubber) temperature–frequency viscoelastic shift factor a_T of compound A. This leads to the friction master curve shown in figure 9 where the coefficient of friction is shown as a function of the logarithm of the sliding velocity at the reference temperature $T = 20\,^\circ$C.

The surface roughness of the road sample used in the experiment has been measured with 1D stylus line scan and 2D optical methods. We have then calculated the surface roughness top power spectrum from the measured topography and combined the two results into a broader power spectrum, see figure 7 (red curve). Note how the two power spectra join smoothly at $q \approx 10^{4.7}$ m^{-1}.

In section 4 we describe in more detail how the viscoelastic modulus of the rubber is measured.

3. Theory

Figure 1 shows the basic picture used in analyzing the rubber friction problem: Many length scales are involved

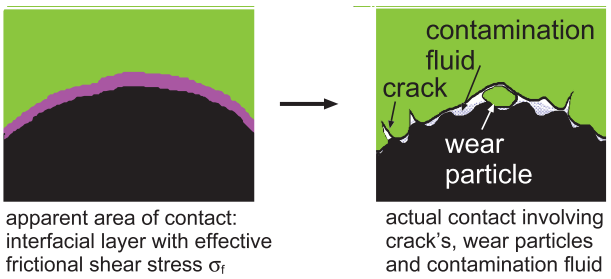

Figure 2. The interfacial wear layer (left) may involve highly non-linear processes (right) e.g., crack propagation, wear particles, fluid contamination layers or, more microscopically, adhesion of rubber molecules followed by stretching and snap off or interfacial crack propagation. All these processes will (during sliding) result in energy dissipation, and will contribute to the effective shear stress τ_f.

and the friction has contributions from all the length scales. The viscoelastic contribution to the friction arises from the (time-dependent) deformations of the rubber by all the different sized asperities, which can be observed as the magnification increases up to the cut-off ζ_1. When the contact regions are observed at a magnification larger than ζ_1 the interfacial stress (and temperature) becomes so high that highly non-linear processes, such as bond breaking and wear processes, will occur, which cannot be described using continuum (viscoelastic) theory, but which may require an atomistic approach. These regions are indicated by the pink area in the figure, and we will refer to this as the interfacial wear layer. The effective frictional shear stress which acts on the wear layer in the contact regions is denoted by τ_f, and will in general depend on the sliding velocity and the temperature. The friction force

$$F_f = F_{visc} + \tau_f(v)A(v) \tag{1}$$

where F_{visc} is the viscoelastic contribution to the friction and $\tau_f(v)A(v)$ the contribution from the area of contact, $A(v)$, which depends strongly on the sliding velocity. If $F_0 = A_0\sigma_0$ denotes the normal force, the friction coefficient

$$\mu = \frac{F_{visc}}{F_0} + \frac{\tau_f(v)}{\sigma_0}\frac{A(v)}{A_0}.$$

Understanding the origin of τ_f may require insight into bond breaking (wear) and other atomistic processes occurring in the contact area (see figure 2). In the study reported on in [21] we attributed τ_f for unfilled rubber to the shearing of a thin confined (smear) film, and for filled rubber to energy dissipation at the opening cracks at the exit of the asperity contact regions.

The basic equations used to calculate $F_{visc}(v)$ and $A(v)$ are presented in [5, 6, 21, 31]. The theory takes into account the frictional heating in the road asperity rubber contact regions (flash temperature) by solving the heat diffusion equations in an approximate way (see [6]).

4. Viscoelastic modulus

To calculate the rubber friction we need the effective rubber bulk viscoelastic modulus $E(\omega)$ for large strain (of order

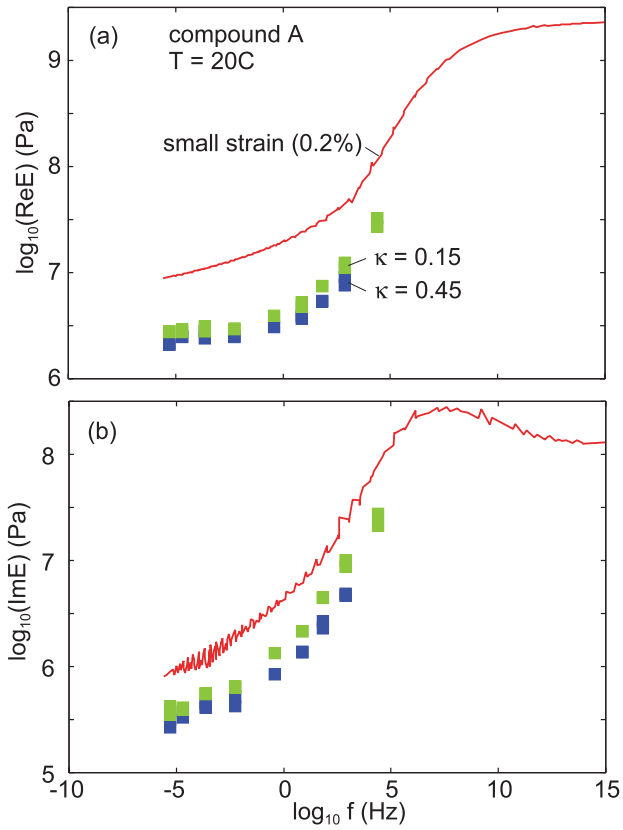

Figure 3. The real (a) and imaginary (b) part of the viscoelastic modulus as a function of frequency, as obtained using experimental data for compound A. The reference temperature is $T = 20\,^{\circ}C$, and the red curve shows the results measured at small strain (0.2%). The green and blue squares are large strain or stress results obtained from strain-sweep data using the self-consistent stress procedure (equation (13)) with $\kappa = 0.15$ (green symbols) and $\kappa = 0.45$ (blue symbols).

100%) and in this section we describe how we have obtained $E(\omega)$. From the viscoelastic modulus measured at small strain (0.2%) for frequencies $f = 0.5, 1.6, 5.0, 15.8, 50.0$ Hz, and for many temperatures between $T = -60\,^{\circ}C$ and $T = 120\,^{\circ}C$, we have obtained a smooth master curve by shifting the frequency segments of the real part of $E(\omega)$. The results for $\mathrm{Re}\,E(\omega)$ and $\mathrm{Im}\,E(\omega)$ are shown (without smoothing) by the red lines in figure 3. The corresponding shift function a_T is shown in figure 4.

Next, to obtain the effective (large strain or stress) viscoelastic modulus, to be used in most contact mechanics applications, we have performed strain sweeps at different temperatures and at fixed frequency (1 Hz). We shift these measured data using the shift function a_T obtained at small strain (figure 4). That this is a reasonable procedure has been shown in other (unpublished) measurements [32], but this is also consistent with the results presented below, where a smooth master curve at large strain is obtained using this procedure. We have developed a procedure (for the software, see www.MultiscaleConsulting.com) from which the effective large-strain (or large stress) viscoelastic modulus can be determined for any given strain or stress amplitude by interpolation of the strain sweeps. However, the most

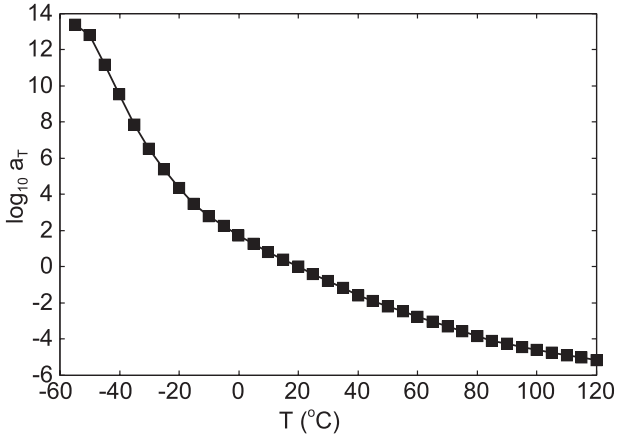

Figure 4. The shift factor a_T as a function of the temperature T. The reference temperature $T = 20\,^{\circ}\mathrm{C}$.

relevant $E_{\mathrm{eff}}(\omega)$ to be used in contact mechanics application will involve varying stress or strain amplitudes, as we now discuss in detail.

The relative contact area when a viscoelastic solid (with a flat surface) is sliding on a randomly rough (hard) substrate surface is given by (from [5]):

$$\frac{A}{A_0} = \frac{2}{\pi}\int_0^\infty \mathrm{d}x\, \mathrm{e}^{-x^2 G(q)} \tag{2}$$

where

$$G(q) = \frac{1}{8}\int_{q_L}^{q} \mathrm{d}^2q'\, q'^2 C(q')\frac{1}{2\pi}\int_0^{2\pi}\mathrm{d}\phi\, \left|\frac{E(q'v\cos\phi)}{(1-\nu^2)\sigma_0}\right|^2 \tag{3}$$

where σ_0 is the normal nominal stress. The dominant contribution to this integral is usually the large wavevector $q' \approx q$ region, and we can approximate

$$G(q) \approx \frac{1}{8}\left|\frac{E(\omega)}{(1-\nu^2)\sigma_0}\right|^2 \int_{q_L}^{q} \mathrm{d}^2q'\, q'^2 C(q') \tag{4}$$

where $\omega = qv$. The average (rms) surface slope $\kappa(q)$ including the surface roughness wavevector components with wavevector $|\mathbf{q}| < q$ is determined by

$$\kappa^2(q) = \int_{q_L}^{q} \mathrm{d}^2q'\, q'^2 C(q'). \tag{5}$$

Thus

$$G(q) \approx \frac{|E(\omega)|^2}{8(1-\nu^2)^2\sigma_0^2}\kappa^2(q). \tag{6}$$

When the contact area $A \ll A_0$ equation (2) reduces to [5]:

$$\frac{A}{A_0} \approx [\pi G(q)]^{-1/2}. \tag{7}$$

Using (6) this gives

$$\frac{A}{A_0} \approx \left(\frac{8}{\pi}\right)^{1/2}\frac{\sigma_0(1-\nu^2)}{|E(\omega)|}\kappa^{-1}(q). \tag{8}$$

Using that $\sigma A = \sigma_0 A_0$ we get

$$\frac{\sigma_0}{\sigma} \approx \left(\frac{8}{\pi}\right)^{1/2}\frac{\sigma_0(1-\nu^2)}{|E(\omega)|}\kappa^{-1}(q) \tag{9}$$

or

$$\sigma \approx \left(\frac{\pi}{8}\right)^{1/2}\frac{|E(\omega)|}{(1-\nu^2)}\kappa(q). \tag{10}$$

For $\kappa \to 0$, $\sigma \to \sigma_0$, and we can interpolate between this limit and the small contact area limit where $\sigma \gg \sigma_0$ using

$$\sigma \approx \sigma_0 + \left(\frac{\pi}{8}\right)^{1/2}\frac{|E(\omega)|}{(1-\nu^2)}\kappa(q). \tag{11}$$

Now real rubber is non-linear and we can take this approximately into account by replacing $E(\omega)$ with an effective modulus which depends on the stress: $E = E(\omega, \sigma)$. This gives

$$\sigma \approx \sigma_0 + \left(\frac{\pi}{8}\right)^{1/2}\frac{|E(\omega,\sigma)|}{(1-\nu^2)}\kappa(q). \tag{12}$$

Exact numerical studies have shown that the factor $(\pi/8)^{1/2}$ should be replaced by $\approx$0.5 (see [33–37]). For rubber materials $\nu \approx 0.5$. Thus we can write

$$\sigma \approx \sigma_0 + 0.67\kappa|E(\omega,\sigma)|. \tag{13}$$

In most applications $\sigma \gg \sigma_0$, so the strain involved in the asperity contact regions will be of order $\sigma/|E(\omega,\sigma)| \approx 0.67\kappa$ and, since typically (for road surfaces) $\kappa \approx 1$, the strain will typically be of order unity.

Equation (13) is an implicit equation for σ, and hence for $E(\omega,\sigma)$, which can be solved, e.g., by iteration. We will denote the resulting $E_{\mathrm{eff}}(\omega) = E(\omega,\sigma)$ as the effective elastic modulus obtained for the self-consistent stress σ. We believe that E_{eff} is the most relevant elastic modulus in contact mechanics between surfaces with roughness on many length scales.

Figure 3 shows the real (a) and the imaginary (b) part of the viscoelastic modulus as a function of frequency, as obtained using experimental data for compound A. The reference temperature is $T = 20\,^{\circ}\mathrm{C}$ and the red curve is the small (0.2%) strain result. The green and blue squares are large strain or stress results obtained from the strain-sweep data using the self-consistent stress procedure (equation (13)) with $\kappa = 0.15$ (green symbols) and $\kappa = 0.45$ (blue symbols). The low-strain curves have been obtained by shifting the real part of the modulus E and the large-strain results (performed at different temperatures) have been shifted using the shift factor a_T obtained from the low-strain calculation.

Figure 5 shows tangent delta ($\tan\delta$) as a function of frequency, as obtained using experimental data for compound A. The temperature $T = 20\,^{\circ}\mathrm{C}$ and the red curve is for small strain. The green and blue squares are the large strain or stress results obtained from strain-sweep data using the self-consistent stress procedure with $\kappa = 0.15$ (green symbols) and $\kappa = 0.45$ (blue symbols).

Figure 6 shows similar results as in figure 3 but for a surface with higher rms slope, $\kappa = 0.7$. The solid lines are again the low-strain (0.2%) results, and the square symbols the

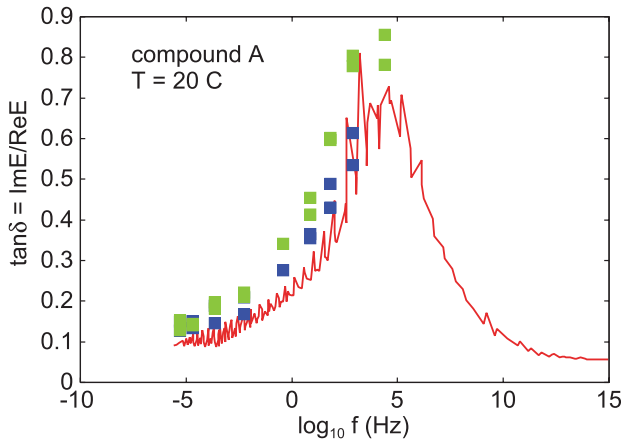

Figure 5. Tangent delta ($\tan\delta$) as a function of frequency, as obtained using experimental data for compound A. The temperature $T = 20\,^{\circ}$C and the red curve is for small strain (0.2%). The green and blue squares are large strain or stress results obtained from strain-sweep data using the self-consistent stress procedure with $\kappa = 0.15$ (green symbols) and $\kappa = 0.45$ (blue symbols).

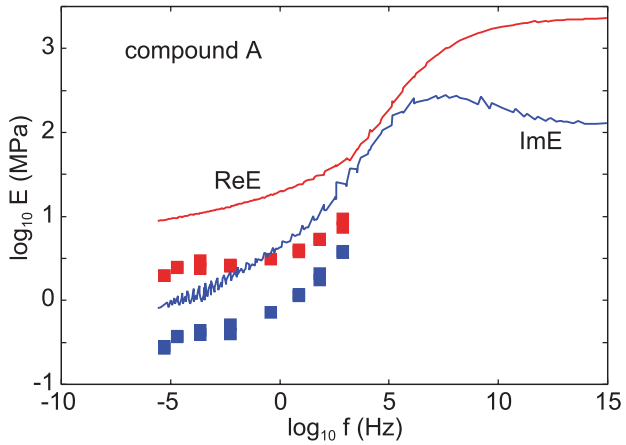

Figure 6. The logarithm of the real (red) and imaginary (blue) part of the viscoelastic modulus as a function of the logarithm of the frequency of compound A at the reference temperature $T_0 = 20\,^{\circ}$C. The square symbols have been obtained at the self-consistent stress given by equation (13) for a rough surface with the rms slope $\kappa = 0.7$.

large-strain results, obtained at the self-consistent stress given by equation (13). All results are at the reference temperature $T_0 = 20\,^{\circ}$C. In the calculations presented below we have used the large-strain results (squares) for the frequency range measured, while for higher frequencies we have used a smooth extrapolation based on the small-strain results. In the future strain sweeps should be performed at lower temperatures in order to extend the measurements of the large-strain viscoelastic modulus to higher frequencies. However, the instrument we used for measuring the viscoelastic modulus cannot apply a large enough force for lower temperatures.

5. Numerical results and comparison with experiment

We will now use the effective viscoelastic modulus obtained above (figure 6) to calculate how the friction depends on the sliding velocity. We assume that there are two contributions to the friction, one from the viscoelastic deformations of the rubber surface by the road asperities, and one from the area of contact. We include in the calculation of the former all the roughness components with wavevectors in the range $q_0 < q < q_1$ with $q_0 = 300\ \mathrm{m}^{-1}$ (which correspond to π/L, where $L \approx 1$ cm is the linear size of the 'tread blocks' used in our measurements of the rubber friction) and $q_1 = 10^6\ \mathrm{m}^{-1}$, corresponding to a short distance cut-off length $d = \pi/q_1 \approx 3\ \mu$m, which is a typical thickness for the wear layer (thickness of the layer of modified rubber on the rubber surface, which we assume acts as a cut-off). In the original rubber friction theory [5] a yield criteria involving the stress and temperature in the asperity contact regions was used to determine q_1, but this procedure has not been extended to the present case, where we include a contribution to the friction from the area of contact.

In what follows, the area of contact is defined as the contact area which results when all the roughness components, $q_0 < q < q_1$, are included in the calculation, i.e., it corresponds to the area observed at the magnification $\zeta = q_1/q_0$. We assume that the frictional shear stress in the area of contact depends weakly on the velocity according to

$$\tau_{\mathrm{f}} = \tau_0(a_T v)^{\alpha},$$

where a_T is the temperature–frequency viscoelastic shift factor. If v is in units of m s^{-1} then we find, using $\tau_0 = 2.1$ MPa and $\alpha = 0.05$, good agreement with experiments. Note that we assume that the frictional shear stress depends on temperature (via a_T) according to the bulk viscoelastic modulus. Only if this is the case will the total friction obey the same temperature–frequency (or velocity) scaling as the bulk viscoelastic modulus. This scaling has been observed in our friction measurements, and in several earlier studies, e.g., by Grosch [38]. This indicates that the frictional shear stress τ_{f} in the area of contact is mainly due to processes involving the rubber, e.g., shearing a thin fluid-like film formed by segments of rubber molecules. Another possibility, which we consider unlikely in the present case, is that the frictional shear stress is associated with adhesive crack opening (as we found earlier for filled SB-rubber) or rubber wear processes (e.g. crack propagation removing small rubber particles). The expression we use for the frictional shear stress is very weakly velocity dependent and has been chosen so as to reproduce the measured friction at low velocities. However, the resulting shear stress is very similar to what we found for unfilled SB-rubber in an earlier study, see [21], where the frictional shear stress in the area of contact was interpreted as due to shearing of a nanometer thick confined fluid-like layer [23, 24] (see footnote 1), [26]. Nevertheless, more combined experimental–theory studies are necessary in order to gain a better insight into the nature of the shear stress in the area of contact.

We first show results for the friction coefficient for the asphalt road surface 1 with the power spectrum shown in figure 7 (red line). For this surface we show in figure 8 the root-mean-square surface slope κ as a function of $\log_{10}q$, where q is the largest (cut-off) wavevector of the roughness included in the calculation of κ.

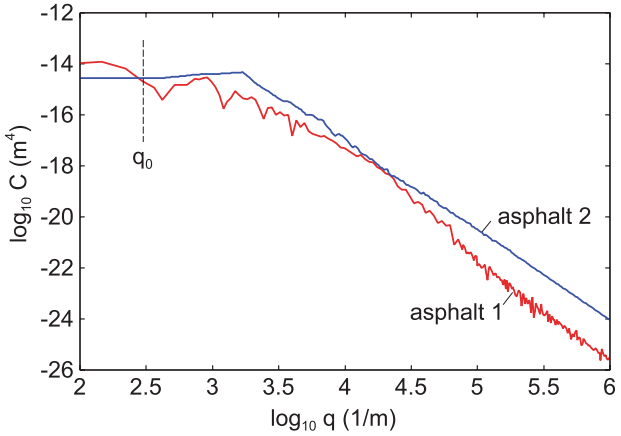

Figure 7. The power spectrum for two asphalt road surfaces, as a function of the wavevector q ($\log_{10} - \log_{10}$ scale). The vertical dashed lines indicate the cut-off wavevector q_0.

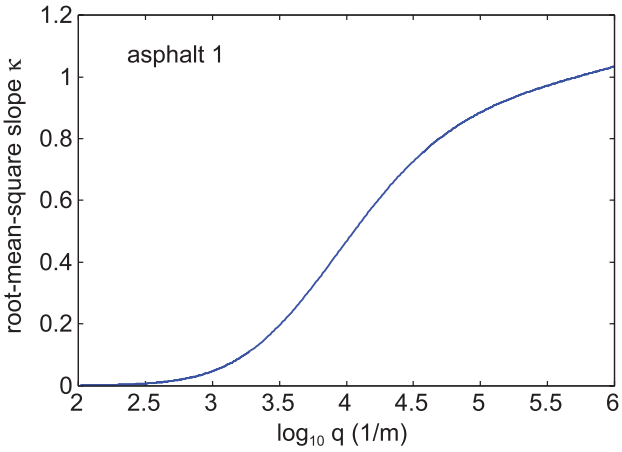

Figure 8. The root-mean-square surface slope κ for the asphalt 1 surface as a function of $\log_{10} q$, where q is the largest (cut-off) wavevector of the roughness included in the calculation of κ.

In figure 9 we show, for compound A at $T_0 = 20\,^{\circ}\mathrm{C}$, the measured (squares) and the calculated (solid lines) friction coefficient as a function of the logarithm of the sliding velocity. The green line is the total calculated friction coefficient, while the blue and pink lines are the viscoelastic contribution and the contribution from the area of contact, respectively. The dashed lines are with the flash temperature effect included and the solid lines without the flash temperature.

We note that in order to correctly reproduce the measured friction at different temperatures ($-8\,^{\circ}\mathrm{C}$, $20\,^{\circ}\mathrm{C}$ and $48\,^{\circ}\mathrm{C}$) it is necessary to assume that the frictional shear stress in the area of contact depends on the temperature (via the shift factor a_T) in the same way as the bulk viscoelastic modulus. In figure 10 the calculated friction coefficient is shown as a function of the logarithm of the sliding velocity for compound A. The red, green and blue lines are for the temperatures $T = 10\,^{\circ}\mathrm{C}$, $30\,^{\circ}\mathrm{C}$ and $60\,^{\circ}\mathrm{C}$, respectively. The dashed lines include the flash temperature while the solid lines represent results without the flash temperature effect.

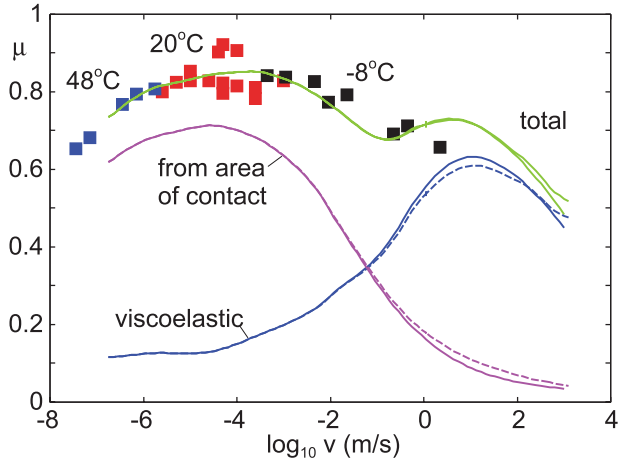

Figure 9. The measured (squares) and the calculated (solid lines) friction coefficient as a function of the logarithm of the sliding velocity for compound A at $T_0 = 20\,^{\circ}\mathrm{C}$. The green line is the total calculated friction coefficient and the blue and pink line the viscoelastic contribution and the contribution from the area of contact, respectively. The dashed lines are with the flash temperature included and the solid lines without the flash temperature. The frictional shear stress in the area of contact is assumed to be weakly velocity dependent $\tau_f = \tau_0(a_T v)^{0.05}$, where a_T is the temperature–frequency viscoelastic shift factor (with $a_T = 1$ for $T = 20\,^{\circ}\mathrm{C}$) and if v is in units of m s^{-1} then $\tau_0 = 2.1$ MPa.

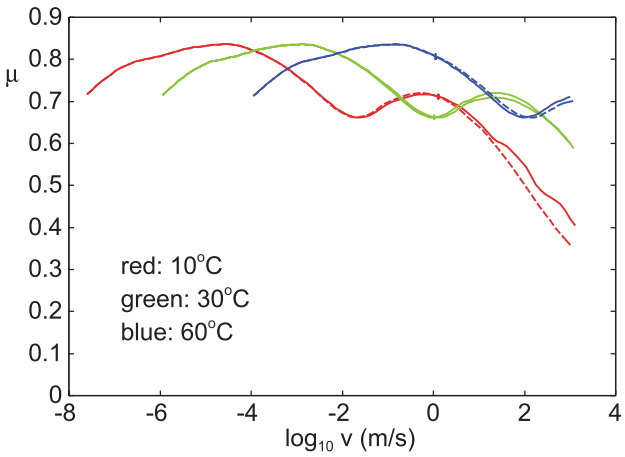

Figure 10. The calculated friction coefficient as a function of the logarithm of the sliding velocity for compound A. The red, green and blue lines are for the temperatures $T = 10\,^{\circ}\mathrm{C}$, $30\,^{\circ}\mathrm{C}$ and $60\,^{\circ}\mathrm{C}$, respectively. The dashed lines include the flash temperature while the solid lines represent results without the flash temperature effect. The frictional shear stress in the area of contact is assumed to be weakly velocity dependent $\tau_f = \tau_0(a_T v)^{0.05}$, where a_T is the temperature–frequency viscoelastic shift factor (with $a_T = 1$ for $T = 20\,^{\circ}\mathrm{C}$) and if v is in units of m s^{-1} then $\tau_0 = 2.1$ MPa.

The road surface used in the calculation above is rather 'smooth'. In figure 7 we show the power spectrum for this and another road surface (asphalt 2). For the more rough (or open) asphalt 2 the contribution to the total friction from the area of contact is smaller while the viscoelastic contribution is larger than for the surface used above. This is illustrated in figure 11, which shows (for compound A at $T_0 = 30\,^{\circ}\mathrm{C}$) the calculated friction coefficient as a function of the logarithm of the sliding

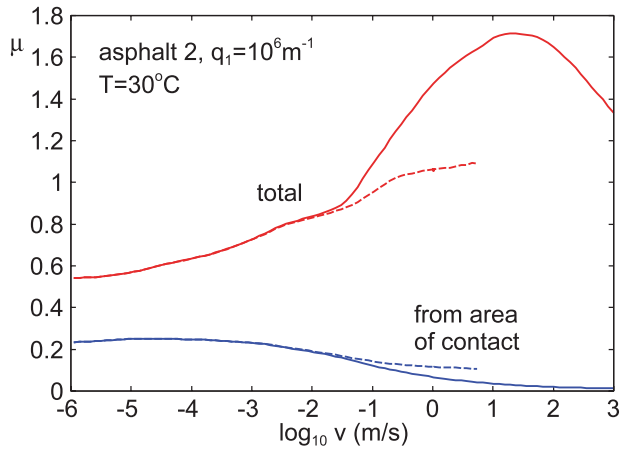

Figure 11. The calculated friction coefficient as a function of the logarithm of the sliding velocity for the asphalt 2 road surface. For $T_0 = 30\,^{\circ}\mathrm{C}$. The upper curves are the total friction and the lower curves the contribution from the area of contact. The dashed lines is with the flash temperature included and the solid lines without the flash temperature. The frictional shear stress in the area of contact is assumed to be weakly velocity dependent $\tau_f = \tau_0(a_T v)^{0.05}$, where a_T is the temperature–frequency viscoelastic shift factor (with $a_T = 1$ for $T = 20\,^{\circ}\mathrm{C}$). If v is in units of m s^{-1} then $\tau_0 = 2.1$ MPa.

velocity for the asphalt 2 road surface. The upper curves are the total friction and the lower ones the contribution from the area of contact. The dashed lines are again with the flash temperature effect included and the solid lines without it. The frictional shear stress in the area of contact is assumed to be weakly velocity dependent $\tau_f = \tau_0(a_T v)^{0.05}$, where a_T is the temperature–frequency viscoelastic shift factor (with $a_T = 1$ for $T = 20\,^{\circ}\mathrm{C}$) and if v is in units of m s^{-1} then $\tau_0 = 2.1$ MPa.

6. Discussion

Let us compare the results presented above with the study presented in [21] for unfilled and filled SB-rubber. We note first that the tread compound used above has similar viscoelastic properties to the unfilled SB-rubber used in [21], but is very different from the filled (with carbon black) SB-rubber. This is consistent with the observed frictional properties for the compound used above, which are similar to that of the unfilled SB-rubber. Thus, in both cases the friction can be explained as the sum of the viscoelastic contribution and a contribution from the area of contact resulting from shearing of a thin (a few nanometers thick) confined film, most likely derived from the rubber (rubber chain segments). In contrast, for the filled SB-rubber, the velocity dependency of the effective shear stress in the area of real contact was very strong, and we attributed this contribution to viscoelastic deformations of the rubber at the opening cracks at the exit of the asperity contact regions. In this case we also observed rubber wear consisting of a dry powder of wear particles rather than a smear film as for the unfilled SB-rubber. Of course, there may also have been a contribution from shearing a thin confined film in the area of contact for the filled SB-rubber, but this contribution would be small because of the much smaller area of contact for the filled SB-rubber–road system studied in [21], as compared to the present systems, and also compared to the case of unfilled SB-rubber. This difference in the sliding properties between the system studied above, and the filled SB-rubber, also manifested itself as follows: In [21] we found that adding a small amount of a high-viscosity silicon oil (viscosity 1 Pa) reduced the friction (at the sliding velocity $\sim$0.1 mm s^{-1}) by more than a factor of 2. We interpreted this as resulting from the fluid-induced removal of the adhesive rubber–substrate interaction, which also removes the contribution from the opening cracks. In the present case, adding a small amount of the same silicon oil had only a very small influence on the sliding friction (it dropped by less than $\sim$5%) at similar sliding velocities ($\sim$0.1 mm s^{-1}). We attribute this small effect on the friction to the fact that the silicon oil is nearly fully removed (squeezed out) from the contact regions at the small sliding velocity, resulting in a nanometer thick confined film. Here we note that water has a viscosity about 1000 times smaller than the silicon oil we have used, and it is known that a thin water film at sliding velocities $\sim$0.1 m s^{-1} (i.e. 1000 times higher than in the present experiment) on road surfaces has a negligible influence on the sliding friction, which is consistent with our observation.

Our study shows that the experimental friction data at $-8\,^{\circ}\mathrm{C}$, $20\,^{\circ}\mathrm{C}$ and $48\,^{\circ}\mathrm{C}$, when shifted by the measured bulk viscoelastic shift factor a_T, forms a smooth master curve, which agrees rather well with the calculated results. Figure 9 shows that for low sliding velocities the dominant contribution to the friction arises from the area of contact while for high velocities the viscoelastic contribution dominates. The rapid drop in the contribution from the area of contact is due to the fact that the area of contact drops when the velocity increases. This is a result of the fact that when the pulsating frequencies from the asperity interaction increase, the effective elastic modulus of the rubber increases. We also note that the dependency of the area of contact on the velocity is not so accurate for high velocities due to the limited frequency range in which the large stain viscoelastic modulus has been measured (see squares in figure 6). When the flash temperature is included (dashed lines) the area of contact at high velocities increases. This is expected since increasing temperature shifts the viscoelastic spectrum to higher frequencies and the rubber becomes effectively elastically softer. The results in figure 10 show that, neglecting the influence of the flash temperature, the friction at different temperatures has a similar velocity dependency but is shifted along the velocity axis in accordance with the bulk viscoelastic shift factor a_T. This is also what is found in experiments performed at such low velocities that frictional heating can be neglected (see above).

7. Summary and conclusion

We have studied the friction force on a rubber block sliding on an asphalt road surface. The friction coefficient measured at three different temperatures in a large velocity range could be shifted to form a smooth master curve using the temperature–frequency shift factor a_T obtained from

measurements of the bulk viscoelastic modulus. We have analyzed the data using a model where the friction consists of a viscoelastic deformation part due to the interaction with the road asperities and a contribution from shearing the area of contact. At low velocities, and for the relatively smooth road surface used, we find that the contribution from the area of contact dominates, while at higher sliding velocities the asperity deformation contribution dominates. We interpret the contribution to the friction from the area of contact as originating from shearing of a thin (nanometer) confined film, probably a rubber smear film.

We have developed a new procedure to obtain the viscoelastic modulus of rubber, where the large-strain modulus is obtained from a combination of low-strain measurements and strain sweeps to large strain performed at a fixed frequency but different temperatures. The large-strain modulus gives a very similar viscoelastic contribution to the calculated rubber friction as obtained using the small-strain measured modulus because both the real and imaginary part of the modulus are reduced in a similar way when the strain increases, and the viscoelastic contribution basically scales with $\mathrm{Im}\, E/|E|$. However, the calculated area of real contact increases a lot (typically by a factor of 5–10) when the large-strain modulus is used, and it is very important to use the (correct) large-strain modulus, in particular at low sliding velocities. With increasing sliding velocity the area of contact rapidly decreases because the rubber appears stiffer at the higher pulsating asperity-interaction frequencies it is exposed to at higher velocities. This explains why the contribution from the area of real contact is most important at low sliding velocities. More combined experimental–theory studies should be performed in order to test the picture of rubber friction obtained in this work and in [21].

References

[1] Persson B N J 2000 *Sliding Friction: Physical Principles and Applications* 2nd edn (Heidelberg: Springer)
[2] Grosch K A 1963 *Proc. R. Soc. Lond.* A **274** 21
[3] Gent A N and Walter J D (ed) 2006 The pneumatic tire *US Department of Transportation Report*
[4] Pacejka H B 2006 *Tyre and Vehicle Dynamics* 2nd edn (Amsterdam: Elsevier)
[5] Persson B N J 2001 *J. Chem. Phys.* **115** 3840
[6] Persson B N J 2006 *J. Phys.: Condens. Matter* **18** 7789
[7] Heinrich G, Klüppel M and Vilgis T A 2000 *Comput. Theor. Polym. Sci.* **10** 53
[8] Heinrich G and Klüppel M 2008 *Wear* **265** 1052
[9] Klüppel M and Heinrich G 2000 *Rubber Chem. Technol.* **73** 578
[10] Westermann S, Petry F, Boes R and Thielen G 2004 *Kautsch. Gummi Kunstst.* **57** 645
[11] Persson B N J and Volokitin A I 2006 *Eur. Phys. J.* E **21** 69
[12] Carbone G, Lorenz B, Persson B N J and Wohlers A 2009 *Eur. Phys. J.* E **29** 275
[13] Persson B N J 1998 *Surf. Sci.* **401** 445
[14] Le Gal A and Klüppel M 2005 *J. Chem. Phys.* **123** 014704
[15] Persson B N J 2009 *J. Phys.: Condens. Matter* **21** 485001
[16] Mofidi M, Prakash B, Persson B N J and Albohr O 2008 *J. Phys.: Condens. Matter* **20** 085223
[17] See, e.g. Persson B N J, Albohr O, Tartaglino U, Volokitin A I and Tosatti E 2005 *J. Phys.: Condens. Matter* **17** R1
[18] Persson B N J, Albohr O, Creton C and Peveri V 2004 *J. Chem. Phys.* **120** 8779
[19] Persson B N J 2011 *J. Phys.: Condens. Matter* **23** 015003
[20] Persson B N J 2010 *Eur. Phys. J.* E **33** 327
[21] Lorenz B, Persson B N J, Dieluweit S and Tada T 2011 *Eur. Phys. J.* E **34** 129
[22] Busse L, Boubakri I and Klüppel M 2011 *Kautsch. Gummi Kunstst.* **64** 35
[23] Sivebaek I, Samolilov V and Persson B N J 2012 *Phys. Rev. Lett.* **108** 036102
[24] Yamada S 2002 *Tribol. Lett.* **13** 167
[25] Yew Y K, Minn M, Sinha S K and Tan V B C 2011 *Langmuir* **27** 5891
[26] Sivebaek I, Samolilov V and Persson B N J 2008 *Eur. Phys J* E **27** 37
[27] Persson B N J and Brener E 2005 *Phys. Rev.* E **71** 036123
[28] Persson B N J, Albohr O, Heinrich G and Ueba H 2005 *J. Phys.: Condens. Matter* **17** R1071
[29] Carbone G and Mangialardi L 2004 *J. Mech. Phys. Solids* **52** 1267
[30] Williams M L, Landel R F and Ferry J D 1955 *J. Am. Chem. Soc.* **77** 3701
[31] Persson B N J 2006 *Surf. Sci. Rep.* **61** 201
[32] Tada T 2011 private communication
[33] Persson B N J 2008 *J. Phys.: Condens. Matter* **20** 312001
[34] Yang C and Persson B N J 2008 *J. Phys.: Condens. Matter* **20** 215214
[35] Hyun S, Pei L, Molinari J-F and Robbins M O 2004 *Phys. Rev.* E **70** 026117
[36] Campana C and Müser M H 2004 *Europhys. Lett.* **70** 026117
[37] Almqvist A, Campañá C, Prodanov N and Persson B N J 2011 *J. Mech. Phys. Solids* **59** 2355
[38] Grosch K A 1997 *Rubber Chem. Technol.* **69** 495